Check for updates

View Article Online
View Journal

PCCP

Accepted Manuscript

This article can be cited before page numbers have been issued, to do this please use: Y. Wang and Y. Ding, *Phys. Chem. Chem. Phys.*, 2017, DOI: 10.1039/C7CP03250A.

This is an Accepted Manuscript, which has been through the Royal Society of Chemistry peer review process and has been accepted for publication.

Accepted Manuscripts are published online shortly after acceptance, before technical editing, formatting and proof reading. Using this free service, authors can make their results available to the community, in citable form, before we publish the edited article. We will replace this Accepted Manuscript with the edited and formatted Advance Article as soon as it is available.

You can find more information about Accepted Manuscripts in the author guidelines.

Please note that technical editing may introduce minor changes to the text and/or graphics, which may alter content. The journal's standard Terms & Conditions and the ethical guidelines, outlined in our author and reviewer resource centre, still apply. In no event shall the Royal Society of Chemistry be held responsible for any errors or omissions in this Accepted Manuscript or any consequences arising from the use of any information it contains.

ROYAL SOCIETY OF CHEMISTRY

rsc.li/pccp

View Article Online
DOI: 10.1039/C7CP03250A

Journal Name

ARTICLE TYPE

Cite this: DOI: 10.1039/xxxxxxxxxx

Structural Stability and Electronic Properties of $(SiH)_2O$-formed Siloxene Sheet: A Computational Study

Yanli Wang*[a], and Yi Ding*[b]

Received Date
Accepted Date

DOI: 10.1039/xxxxxxxxxx

www.rsc.org/journalname

Very recently, a $(SiH)_2O$-formed siloxene sheet has been synthesized in the experiment [S. Li, *et al.* J. Mater. Chem. A 2016, **4**, 15841]. Utilizing first-principles calculations, we have systematically investigated the structural stability and physical properties of this $(SiH)_2O$ sheet. We have found the dynamically stable structure for it is a puckered one with bent Si-O-Si connections, which leads to an anisotropic elastic behaviour with negative Poisson ratios. The $(SiH)_2O$ sheet has a strain-tunable direct band gap whose valence and conduction band edges straddle the redox potentials of water even in the presence of stress (either tensile or compressive). The calculated carrier mobilities are prominently anisotropic: in its zigzag direction the electron mobility reaches a high value of 5.39×10^3 cm^2/Vs, while the hole mobility remains small. These different carrier mobilities permit fast charge separation and transfer, what is crucial for efficient solar-to-electric energy conversion for photovoltaic and water splitting applications. Similar to phosphorene, a typical linear dichroism phenomenon is also present in the $(SiH)_2O$ sheet. Due to its outstanding electronic properties, the $(SiH)_2O$ sheet is a promising material in the fields of nano-electronics, sustainable energy and fuel generation.

1 Introduction

Analogue to graphene[1,2], the discovery of silicene brings plenty of two-dimensional (2D) Si-based derivatives. The pristine silicene sheet is a buckled Si honeycomb lattice[3–5], which can be fully hydrogenated as a silicane sheet, i.e. the Si analogue of graphane[6–8]. Similar fluorosilicene, chlorosilicene and other halogen-functionalized silicene sheets have also been proposed[9–12], which can be further transformed to the Janus silicane by asymmetrical functionalizations[13,14]. Owing to the substrate effect, one-side functionalization is realized on the silicene sheet[15,16]. In the experiment, the half-silicane sheet, i.e. semi-hydrogenated silicene, has been synthesized on the Ag surface[17]. Besides these silicane-like systems, other Si-based novel nanostructures, such as graphyne-like porous silicyne sheets[18–20], oxidation-induced silica sheets[21,22], and monolayer transition-metal silicide[23,24], have also been reported in the literature.

Very recently, a siloxene sheet has been synthesized in the experiment[25]. The name of siloxene corresponds to a compound with the stoichiometric ratio of Si:H:O=2:2:1. In the previous works, the siloxene sheet is normally regarded as a Janus silicane sheet that has asymmetrical H- and OH-decorations on the two sides of Si basal plane[26,27]. Different buckled structures, such as the chair-like one, washborad case, have been studied for the siloxene sheets in previous literature[28]. However, these H/OH co-decorated structural models are inconsistent with the latest experimental result, which only shows the Si-Si, Si-O, and Si-H vibration signals in the Raman spectra of siloxene[25]. The experimenters have inferred that all the H atoms are directly bonded

[a] *Department of Physics, Center for Optoelectronics Materials and Devices, Zhejiang Sci-Tech University, Xiasha College Park, Hangzhou, Zhejiang 310018, People's Republic of China. E-mail: wangyanli-04@tsinghua.org.cn*
[b] *Department of Physics, Hangzhou Normal University, Hangzhou, Zhejiang 310036, People's Republic of China. E-mail: dingyi2001@tsinghua.org.cn*

† Electronic Supplementary Information (ESI) available: Fig. S1 The convergence test for the imaginary part of dielectric function versus the k-point sampling. Fig. S2 The pictures for the eigenvector of the lowest unstable mode at the Γ point in the ideal $(SiH)_2O$ sheet. Fig. S3 The orientation-dependent Young modulus and Poisson ratio for the ideal $(SiH)_2O$ sheet. See DOI: 10.1039/b000000x/

Published on 19 June 2017. Downloaded by University of Arizona on 19/06/2017 13:21:07.

Physical Chemistry Chemical Physics Accepted Manuscript

View Article Online
DOI: 10.1039/C7CP03250A

Published on 19 June 2017. Downloaded by University of Arizona on 19/06/2017 13:21:07.

to Si atoms in siloxene, where O atoms lie at the bridge site and connect the SiH zigzag lines[25]. This picture is consistent with the chain model of siloxene, which can be view as a $(SiH)_2O$ sheet[29]. However, there are bare studies on this $(SiH)_2O$ nanostructure, for which some basic information, such as the structural stability, electronic structure, mechanical and optical properties, is still unknown. Thus, in this paper, we perform a comprehensive first-principles investigation on the $(SiH)_2O$ sheet.

2 Methods

The first-principles calculations are performed by the VASP code[30,31], which adopts the plane-wave basis sets with Perdew-Burke-Ernzerhof (PBE) projector augmented wave pseudopotentials. The cut-off energy of plane waves is set to 500 eV, and the k-meshes of $12\times18\times1$ and $15\times21\times1$ are used in the relax and static calculations, respectively. A denser k-mesh of $21\times36\times1$ is used in the optical calculations, which is proved to be sufficiently large for the related properties as shown in Fig. S1 of Supporting Information. A vacuum layer of about 15 Å is used in the calculations. All structural parameters are fully optimized until the maximum residual force is less than 0.005 eV/Å. The structural stability of $(SiH)_2O$ sheet is validated through the phonon calculations and density functional based tight binding molecular dynamics (DFTB-MD) simulations, which are performed by the Phonopy and DFTB+ codes[32,33]. Considering the underestimation of band gap by the PBE functional, a hybrid Heyd-Scuseria-Ernzerhof (HSE) calculation is done by the FHI-aims code[34,35], which uses the HSE06 form with a screening parameter of 0.11 $bohr^{-1}$. In order to well reproduce the experimentally measured gap size, the mixing parameter of short-range exchange is set to 0.43 in the HSE calculations.

3 Results and discussions

Figure 1(a) depicts the geometrical structure of the ideal, though unstable at room temperature (as discussed below), $(SiH)_2O$ sheet after atomic relaxation. The silicon atoms form the zigzag chains interconnected by oxygen atoms and are saturated by hydrogens. The lattice constant along the zigzag direction (l_z) is 3.96 Å, close to that of silicane sheet, 3.89 Å[7]; while the lattice constant along the armchair direction (l_a) is elongated to 8.45 Å due to the formation of linear Si-O-Si connections. The cohesive energy of this ideal $(SiH)_2O$ sheet is -4.04 eV/atom, which is larger than those calculated for silicene and silicane, -3.90 and -3.37 eV/atom, respectively. The siloxene sheet hence is energetically more favourable and stable. Using silicane (SiH) and oxygen (O_2) molecules as references, the formation energy of $(SiH)_2O$ sheet is calculated as $E_{form}=(E_{(SiH)_2O}-2\times E_{SiH}-E_{O2}/2)$, where $E_{(SiH)_2O}$ is the total energy of $(SiH)_2O$ sheet, E_{SiH} is the energy of a Si-H pair in the silicane sheet, and E_{O2} is the energy of an isolated O_2 molecule. Following this definition, the E_{form} of $(SiH)_2O$ system is obtained as -3.90 eV/formula unit (f.u.), indicating the transformation from silicane to siloxene by the oxidation is an exothermic reaction. However, Fig. 1(c) shows that this ideal $(SiH)_2O$ sheet is thermally unstable due to the presence of soft modes in the phonon bands[36], which indicate that critical distortions might appear at room temperature. Following the eigenvectors of soft modes (which is shown in Fig. S2 of supporting information), the $(SiH)_2O$ sheet is relaxed again and the final optimized structure is displayed in Fig. 1(b). It can be seen that the basal plane of $(SiH)_2O$ sheet becomes puckered, in which the bent Si-O-Si connections are alternated up and down along the armchair direction. As a result, the Si-H bonds are tilted, and the lattice constant l_a in the armchair direction is shortened to 8.15 Å while the l_z in the zigzag direction remains unchanged (3.96 Å). Accompanied with such pucker, there is an energy gain of 17 meV/f.u. in the $(SiH)_2O$ sheet. Most importantly, all the soft modes are eliminated in this puckered structure, whose phonon frequencies are all positive as shown in Fig. 1(d). Besides that, the structural stability of this puckered $(SiH)_2O$ sheet is further checked by the DFTB-MD simulation, which uses a Nosé thermostat of 500 K with a time step of 1 fs. A 3×6 supercell of $(SiH)_2O$ sheet with a large size of 24.44×23.76 Å is adopted in the simulations. After 10000 steps, the puckered $(SiH)_2O$ sheet still maintains its structural integrity as shown in Figs. 1(e) and (f). Although some distortions appear in the sheet, there are no broken bonds in the final configuration outcoming from DFTB-MB simulations. Thus, puckered $(SiH)_2O$ sheet possesses robust dynamical and thermal stabilities, which suggests it can sustain the free-standing state under normal conditions in the experiment. In the following, we focus on the physical properties of this puckered $(SiH)_2O$ structure.

Firstly, we investigate the mechanical properties of $(SiH)_2O$ sheet. Utilizing the energy-vs.-strain method[37], the elastic moduli of $(SiH)_2O$ sheet are obtained as $C_{11}=19.3$, $C_{22}=46.1$, $C_{44}=15.3$, and $C_{12}=3.2$ N/m. These values well satisfy the Born-Huang criteria for an orthogonal lattice, which are $C_{11}C_{22}-C_{12}^2>0$ and $C_{11},C_{22},C_{44}>0$. This indicates the mechanical stability of puckered structure, which is consistent with the phonon and DFTB-MD simulated results. Based on these elastic moduli, the in-plane Young modulus E and Poisson ratio ν along an arbitrary angle are calculated as

$$E(\theta)=\frac{C_{11}C_{12}-C_{12}^2}{C_{11}s^4+C_{22}c^4+(\frac{C_{11}C_{12}-C_{12}^2}{C_{44}}-2C_{12})c^2s^2}$$

,

$$\nu(\theta)=-\frac{(C_{11}+C_{22}-\frac{C_{11}C_{12}-C_{12}^2}{C_{44}})c^2s^2-C_{12}(c^4+s^4)}{C_{11}s^4+C_{22}c^4+(\frac{C_{11}C_{12}-C_{12}^2}{C_{44}}-2C_{12})c^2s^2}$$

where $c=cos\theta$ and $s=sin\theta$ (θ is the angle relative to the armchair (x) direction))[37]. As shown in Fig. 2, the E and ν of

This journal is © The Royal Society of Chemistry [year]

Physical Chemistry Chemical Physics Accepted Manuscript

View Article Online
DOI: 10.1039/C7CP03250A

Published on 19 June 2017. Downloaded by University of Arizona on 19/06/2017 13:21:07.

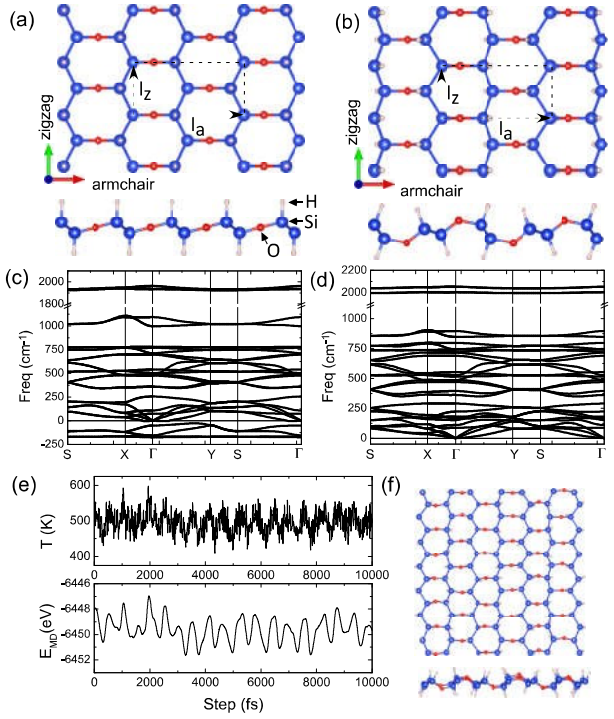

Fig. 1 The geometrical structures of (a) ideal and (b) puckered $(SiH)_2O$ sheets, and [(c), (d)] the corresponding phonon bands for them. (e) The fluctuations of temperature and total energy during the DFTB-MD simulation, and (f) the final structure of the puckered $(SiH)_2O$ sheet after the simulation.

$(SiH)_2O$ sheet are orientation-dependent. Such anisotropic mechanical property is also present in other novel 2D nanomaterials, such as the TiC and Borophenes ones[38,39]. The E has a minimum value of 19.1 N/m in the armchair (x) direction, while the maximum E is 45.6 N/m in the zigzag (y) direction. This value is smaller than the Young moduli of silicene and silicane ($E = 63.8$ and 53.8 N/m[40]), suggesting the $(SiH)_2O$ sheet is a flexible structure. The ν of $(SiH)_2O$ sheet is 0.068 and 0.163 in the x and y directions, respectively, which are also smaller than the values of silicene (0.325) and silicane (0.240)[40]. More interestingly, there are negative Poisson ratios in the $(SiH)_2O$ sheet. As shown in Fig. 2(b), along the $\theta \simeq \pi/4$ direction, the ν value drops to -0.016. This negative ν value means an auxetic behaviour in the system, which will become thicker in the perpendicular direction when the sheet is stretched along the direction with a negative ν[41]. It would be noticed that there is no negative ν reported in silicene and silicane sheets, while the oxidized silicene (SiO) sheet has been found to exhibit an analogue negative Poisson ratio behavior[42]. Both the SiO and $(SiH)_2O$ sheets share similar bent Si-O-Si connections, which form the hinge-like atomic skeleton that renders the auxetic behaviour. Actually, if we adopt the linear Si-O-Si

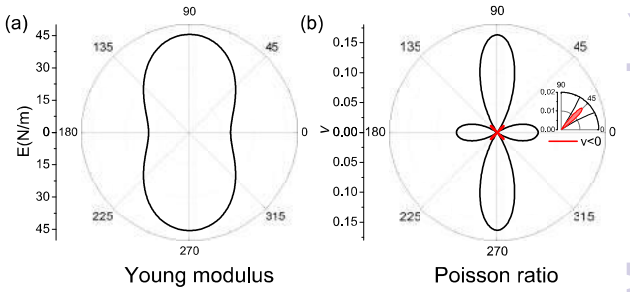

Fig. 2 The orientation-dependent (a) Young modulus (E) and (b) Poisson ratio (ν) for the puckered $(SiH)_2O$ sheet. The region of negative Poisson ratio is zoomed in the inset of (b).

connections as shown in Fig. 1(a), the negative Poisson ratios will disappear in the ideal $(SiH)_2O$ sheet as shown in the Fig. S3 of supporting information.

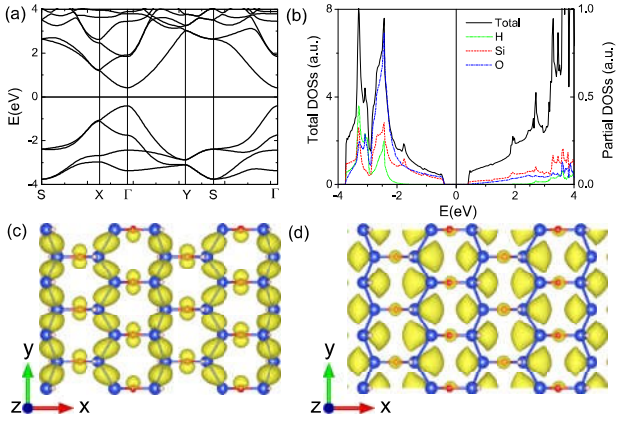

Fig. 3 (a) The band structures and (b) densities of states (DOSs) of $(SiH)_2O$ sheet from the PBE calculations, and the partial charge densities of (c) VBM and (d) CBM for it.

Then, we focus on the electronic properties of puckered $(SiH)_2O$ sheet, whose band structures are depicted in Fig. 3(a). The PBE calculations show the $(SiH)_2O$ sheet has a direct band gap of 0.83 eV, for which the valence band maximum (VBM) and conduction band minimum (CBM) are both located at the Γ point. The corresponding partial density of states (PDOSs) indicate these band edges are mainly contributed by the Si and O atoms. As displayed in Figs. 3(c) and (d), the VBM is constructed by the O p_y and Si p_y orbitals, while the CBM is composed of O p_z and Si p_x ones. The HSE band structures for this $(SiH)_2O$ sheet are depicted in Fig. 4(a), which resemble the PBE ones with a larger band gap of 2.49 eV. Due to the structural anisotropy, the effective masses (m_{eff}) are also anisotropic for the holes and electrons. Based on the HSE results, it can be obtained that for the holes, the m_{eff} is equal to 0.62 m_0 along the $\Gamma - X$ direction

Physical Chemistry Chemical Physics Accepted Manuscript

View Article Online
DOI: 10.1039/C7CP03250A

Published on 19 June 2017. Downloaded by University of Arizona on 19/06/2017 13:21:07.

Physical Chemistry Chemical Physics Accepted Manuscript

while it is reduced to 0.15 m_0 along the $\Gamma-Y$ direction (m_0 is the mass of free electron). For the electrons, the m_{eff} is 0.54 and 0.27 m_0 along the $\Gamma-X$ and $\Gamma-Y$ directions, respectively. The deformation potential constants (E_{DP}) of VBM and CBM, which are calculated as $E_{DP}=|\partial E_{abs}/\partial\varepsilon|$ (E_{abs} is the absolute value of band edges from the HSE calculations, which adopts the vacuum level as the zero point), also exhibit the anisotropic characteristic. Since the VBM is mainly localized in the zigzag Si chains, the y-directional strain will more pronouncedly affect the E_{abs} value than the x-directional strain. Thus, as shown in Tab. 1, a large E_{DP} of 5.63 eV is obtained for the VBM along the y direction, while it is only 3.86 eV along the x direction. Similarly, since the CBM is localized along the x direction but delocalized along the y direction, the E_{DP} of CBM is larger in the x direction than the y direction: 5.40 and 1.34 eV, respectively. Utilizing these data, the carrier mobilities of $(SiH)_2O$ sheet can be estimated by the deformation potential theory[43], which are equal to

$$\mu=\frac{e\hbar^3C}{k_BTm_{eff}m_{ave}E_{DP}^2}$$

. Here, e is the electron charge, $\hbar$ is the reduced Planck constant and k_B is the Boltzmann constant. m_{ave} is the average effective mass, which is calculated as $m_{ave}=\sqrt{(m_{eff})_x(m_{eff})_y}$. As shown in Tab. 1, at room-temperature of T=300 K, for the transport along the x direction, the hole and electron mobilities are both small: 0.14 and 0.13×10^3 cm^2/Vs, respectively. While for the transport along the y direction, the hole mobility increases to 0.67×10^3 cm^2/Vs, and the electron mobility rises to 5.39×10^3 cm^2/Vs. This value is comparable to the high mobilities in phosphorene (1.1-1.14×10^3 cm^2/Vs[43,44]) and GeS monolayer (2.95-3.68×10^3 cm^2/Vs[45]), which is an order of magnitude larger than the carrier mobilities in common transitional metal dichalcogenides (0.34×10^3 cm^2/Vs in MoS_2, 0.24×10^3 cm^2/Vs in $MoSe_2$ and 0.32×10^3 cm^2/Vs in $MoTe_2$[46,47]). Since in the y direction the electron mobility is eight times larger than the hole one, charge separation, and hence transfer, could be extremely efficient for high performance photovoltaic conversion and water splitting devices based on $(SiH)_2O$ sheets, which is consistent with the experimental result[25].

Table 1 The effective masses, deformation potential constants, elastic moduli, and the carrier mobilities of holes and electrons along the x/y direction for the $(SiH)_2O$ sheet under the room-temperature (T=300 K).

		m_{eff} (m_0)	E_{DP} (eV)	C (N/m)	μ (10^3 cm^2/Vs)
hole	x:	0.62	3.86	19.27	0.14
	y:	0.15	5.63	46.08	0.67
electron	x:	0.54	5.40	19.27	0.13
	y:	0.27	1.34	46.08	5.39

Based on the HSE results, optical properties of $(SiH)_2O$ sheet

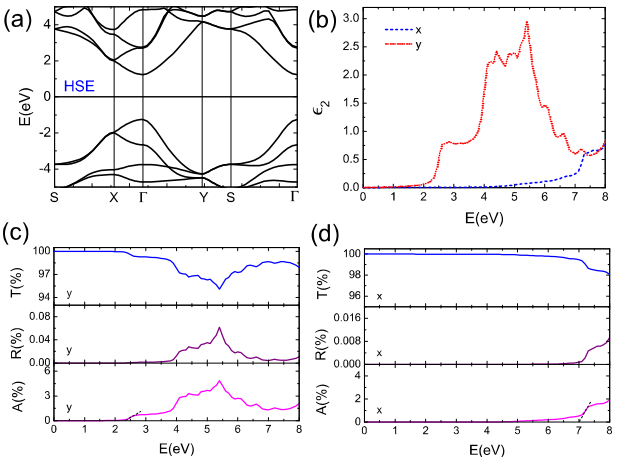

Fig. 4 (a) The band structures and (b) the imaginary part of dielectric function of $(SiH)_2O$ sheet from the HSE calculations. The transmittance, reflectance and absorbance for the incident light polarized in the (c) y and (d) x directions.

are displayed in Figs. 4(c)-(d). Due to the periodic boundary condition, the calculated imaginary part of dielectric function (ε_2) is rescaled by a factor L/d to account for the 2D nature of sheet[48]. L is the used length for the simulated cell, which includes the vacuum layer, while d is the thickness of 2D sheets, which is adopted to the vertical distance between the outside atoms plus their van der Waals atomic radii. As shown in Fig. 4(b), there are remarkable anisotropic characteristics for the ε_2 of $(SiH)_2O$ sheet. For an incident light polarized in the y direction, the first peak of $\varepsilon_2(y)$ appears around the band gap, which extends to 4 eV as a plateau. The $\varepsilon_2(y)$ value continually rises and forms several peaks in the range of [4-6] eV. While for the incident light polarized in the x direction, the $\varepsilon_2(x)$ is always small in the range of [0-6] eV and its first peak appears around 7 eV. The corresponding transmittance (T), reflectance (R) and absorbance (A) of the isolated $(SiH)_2O$ sheet in air are depicted in Figs. 4(c) and (d), which are calculated according to the thin film limit equations: $T=1/(1+\beta n_2/2)^2$, $R=(\beta n_2/2)^2/(1+\beta n_2/2)^2$ and $A=1-T-R$[48]. Here, $\beta=4\pi n_1 d/\lambda$, n_1/n_2 is the real/imaginary part of complex refractive index, d is the thickness of sheet, and λ is wavelength of incident light. It shows the $(SiH)_2O$ sheet can transmit most of the incident light and the reflected light is tiny. Following the process of Qiao *et al.*[43], Figs. 4(c) and (d) indicate the band edge of first absorbance peak is about 2.4 and 7.0 eV for the polarization in the y and x directions. This suggests that similar to phosphorene[43], there is a noticeable linear dichroism in the $(SiH)_2O$ sheet, which is helpful to determine the orientation of nanocrystals.

Finally, we investigate the strain-induced modulation on the electronic structure of $(SiH)_2O$ sheet. In the experiments, utiliz-

View Article Online
DOI: 10.1039/C7CP03250A

Published on 19 June 2017. Downloaded by University of Arizona on 19/06/2017 13:21:07.

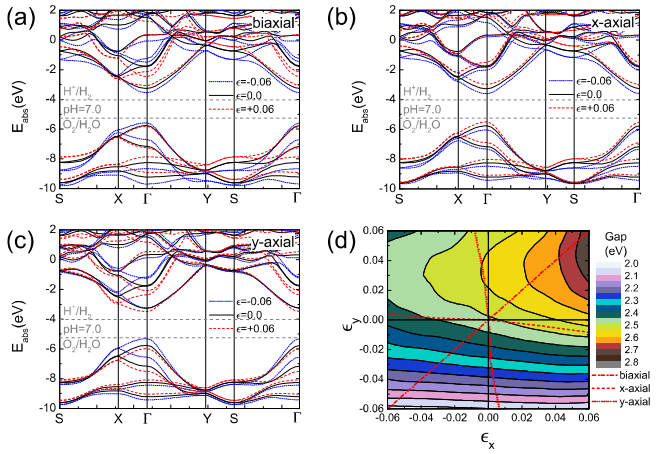

Fig. 5 The HSE band structures of $(SiH)_2O$ sheets under the (a) biaxial strains, (b) x-, and (c) y-directional uniaxial strains. Here, the zero point is adopted to the vacuum level in these strained sheets, and the reduction and oxidation potentials of water under the PH=7 case are marked by dash lines. [d] The band gap of strained $(SiH)_2O$ sheet under the general $(\varepsilon_x, \varepsilon_y)$ strains.

ing different techniques, up to 4% strain can be applied to 2D semiconducting systems[49]. Thus, for the $(SiH)_2O$ sheet, a moderate strain range of $-0.06 < \varepsilon_x, \varepsilon_y < 0.06$ is considered, where $\varepsilon_x = \Delta l_a / l_a$ and $\varepsilon_y = \Delta l_z / l_z$. Figures 5(a)-(c) display the variations of HSE band structures under the biaxial (a) and uniaxial strains along the x and y directions (b,c), respectively. We note that the direct character of the band gap is preserved under stress (either tensile or compressive). The biaxial strain can significantly alter the band gap, which changes from 2.03 eV at $\varepsilon_x = \varepsilon_y = -0.06$ to 2.73 eV at $\varepsilon_x = \varepsilon_y = 0.06$. However, the x-directional uniaxial strain has much less influence on the band gap, which is only varied from 2.43 eV at $\varepsilon_x = -0.06$ to 2.52 eV at $\varepsilon_x = 0.06$. The situation is a little complicated for the y-directional uniaxial strain. It is found that the y-directional compressive strain can remarkably reduce the band gap of $(SiH)_2O$ sheet, which drops to 2.05 eV at $\varepsilon_y = -0.06$, while the y-directional tensile strain has only a negligible effect on the band gap, which is still 2.49 eV at $\varepsilon_y = 0.06$. These diverse strain-modulated behaviours are originated from different responses of band edges to the strain. As shown in Fig. 3(c), the VBM is mainly localized in the zigzag Si chains. Thus, the VBM is sensitive to the y-directional strains, for which the compression would raise the value while the tension lowers it in Fig. 5(c). In contrast, the CBM is delocalized in the zigzag Si chains but localized in the Si-O-Si connections. Thus, a x-directional strain would play a major role on the varation of CBM, which is raised by the tension but drops by the compression. Because the $(SiH)_2O$ sheet has positive Poisson ratios in the x and y directions, a $x(y)$-directional tension/compression will result in a $y(x)$-directional compression/tension. Thus, under uniaxial strains, the VBM and CBM have the same variation trend, which leads to small changes in the band gap. While under the biaxial strains, the VBM and CBM have opposite variation trends, which become closer to each other under the compression and move far away under the tension. This leads to the remarkable band gap variation in the biaxially strained systems. In Fig. 5(d), we further depict the band gaps of $(SiO)_2O$ sheets under a general 2D strain of $(\varepsilon_x, \varepsilon_y)$. The system always has a direct band gap at the Γ point, which is adjustable by straining the 2D system ($\varepsilon_x, \varepsilon_y$ stress). Among the investigated strain range, the maximum band gap reaches up to 2.74 eV under the strain of $(\varepsilon_x = 0.06, \varepsilon_y = 0.05)$, which is 10% larger than the strain-free value, while the minimum gap value is 2.03 eV at $(\varepsilon_x = -0.06, \varepsilon_y = -0.06)$, which is 18 % smaller. We noted that, as shown in Figs. 5(a)-(c), under the biaxial and uniaxial strains, the conduction and valence band edges of $(SiH)_2O$ sheet can always straddle the redox potentials of water. The CBM is above the redox potential of H^+/H_2 (-4.027 eV) under the pH=7 condition, while the VBM is below the redox potential of O_2/H_2O (-5.257 eV). Thus, the band edge positions of $(SiH)_2O$ sheet are suitable for water splitting, which is consistent with the experimental result[25]. Combined the tunable band gap, the $(SiH)_2O$ sheet has many potential applications in nano-electronics and green-energy applications.

4 Conclusion

In summary, we have performed a first-principles study on the structural, mechanical, electronic and optical properties of recently synthesized $(SiH)_2O$-formed siloxene sheet. It has been found that (1) the dynamically stable $(SiH)_2O$ sheet corresponds to a puckered structure, which has robust structural stabilities from the energetic, dynamic, and thermal points of view. (2) This puckered $(SiH)_2O$ sheet has an anisotropic elastic behaviour which can even exhibit an auxetic characteristic with negative Poisson ratios along certain angles. (3) Anisotropic carrier mobilities are obtained in the $(SiH)_2O$ sheet, the electron mobility can reach a high value along the zigzag direction, 5.39×10^3 cm^2/Vs, which is almost one order of magnitude larger than that of holes and which permits fast charge separation and transfer. (4) The $(SiH)_2O$ sheet is a robust direct-gap semiconductor against the strains, whose band-edge levels are suitable for the water splitting in presence of biaxial and uniaxial strains. (5) Besides that, analogous to phosphorene, the typical linear dichroism phenomenon is also present in the $(SiH)_2O$ sheet. Due to these extraordinary electronic properties, this $(SiH)_2O$-formed siloxene sheet will be a promising nanomaterial for nano-electronics and green-energy applications.

Acknowledgements

Authors acknowledge the supports from National Natural Science Foundation of China (11474081), Zhejiang Provincial Natural

Physical Chemistry Chemical Physics Accepted Manuscript

View Article Online
DOI: 10.1039/C7CP03250A

Published on 19 June 2017. Downloaded by University of Arizona on 19/06/2017 13:21:07.

Science Foundation of China (LY15A040008), and Special Program for Applied Research on Super Computation of the NSFC-Guangdong Joint Fund (The Second Phase). The partial calculations were also performed in the Shanghai Supercomputer Center (SSC) of China.

References

1 M. Inagaki and F. Kang, *J. Mater. Chem. A*, 2014, **2**, 13193–13206.
2 Q. Peng, A. K. Dearden, J. Crean, L. Han, S. Liu, X. Wen and S. De, *Nanotechnol. Sci. Appl.*, 2014, **7**, 1–29.
3 L. C. Lew Yan Voon, J. Zhu and U. Schwingenschlogl, *Appl. Phys. Rev.*, 2016, **3**, 040802.
4 J. Zhuang, X. Xu, H. Feng, Z. Li, X. Wang and Y. Du, *Sci. Bull.*, 2015, **60**, 1551–1562.
5 T. Kaloni, G. Schreckenbach, M. Freund and U. Schwingenschlögl, *Phys. Status Solidi RRL*, 2016, **10**, 133–142.
6 J. Kim, M. V. Fischetti and S. Aboud, *Phys. Rev. B*, 2012, **86**, 205323.
7 Y. Ding and Y. Wang, *Appl. Phys. Lett.*, 2012, **100**, 083102.
8 O. D. Restrepo, R. Mishra, J. E. Goldberger and W. Windl, *J. Appl. Phys.*, 2014, **115**, 033711.
9 N. Gao, W. T. Zheng and Q. Jiang, *Phys. Chem. Chem. Phys.*, 2012, **14**, 257–261.
10 F.-b. Zheng and C.-w. Zhang, *Nanoscale Res. Lett.*, 2012, **7**, 1.
11 Q. Jiang, J. Zhang, Z. Ao and Y. Wu, *Sci. Rep.*, 2015, **5**, 15734.
12 W.-B. Zhang, Z.-B. Song and L.-M. Dou, *J. Mater. Chem. C*, 2015, **3**, 3087–3094.
13 P. A. Denis, *Phys. Chem. Chem. Phys.*, 2015, **17**, 5393–5402.
14 M. Sun, Q. Ren, S. Wang, J. Yu and W. Tang, *J. Phys. D: Appl. Phys.*, 2016, **49**, 445305.
15 J. Qiu, H. Fu, Y. Xu, A. I. Oreshkin, T. Shao, H. Li, S. Meng, L. Chen and K. Wu, *Phys. Rev. Lett.*, 2015, **114**, 126101.
16 W. Li, S. Sheng, J. Chen, P. Cheng, L. Chen and K. Wu, *Phys. Rev. B*, 2016, **93**, 155410.
17 W. Wang, W. Olovsson and R. Uhrberg, *Phys. Rev. B*, 2016, **93**, 081406.
18 P. Yang and W. Hai-Bin, *Chin. Phys. B.*, 2013, **22**, 057303.
19 Y. Ding and Y. Wang, *Nanoscale Res. Lett.*, 2015, **10**, 1–11.
20 Y. Zhu, H. Bai and Y. Huang, *J. Phys.: Condens. Matter*, 2016, **28**, 045303–.
21 V. O. Özçelik, S. Cahangirov and S. Ciraci, *Phys. Rev. Lett.*, 2014, **112**, 246803.
22 Y. Han and M. Hu, *Nanotechnology*, 2015, **26**, 505702.
23 A. Manjanath, V. Kumar and A. K. Singh, *Phys. Chem. Chem. Phys.*, 2014, **16**, 1667–1671.
24 N. Han, H. Liu and J. Zhao, *J. Supercond. Novel Magn.*, 2015, **28**, 1755–1758.
25 S. Li, H. Wang, D. Li, X. Zhang, Y. Wang, J. Xie, J. Wang, Y. Tian, W. Ni and Y. Xie, *J. Mater. Chem. A*, 2016, **4**, 15841–15844.
26 G. Vogg, M. S. Brandt, M. Stutzmann and M. Albrecht, *J. Cryst. Growth*, 1999, **203**, 570–581.
27 H. Nakano, M. Ishii and H. Nakamura, *Chem. Commun.*, 2005, 2945–2947.
28 A. Atsalakis and L. Tsetseris, *J. Phys.: Condens. Matter*, 2014, **26**, 285301.
29 P. Deák, M. Rosenbauer, M. Stutzmann, J. Weber and M. S. Brandt, *Phys. Rev. Lett.*, 1992, **69**, 2531–2534.
30 G. Kresse and J. Furthmuller, *Comput. Mater. Sci.*, 1996, **6**, 15–50.
31 G. Kresse and J. Furthmuller, *Phys. Rev. B*, 1996, **54**, 11169–11186.
32 A. Togo and I. Tanaka, *Scr. Mater.*, 2015, **108**, 1–5.
33 B. Aradi, B. Hourahine and T. Frauenheim, *J. Phys. Chem. A*, 2007, **111**, 5678–5684.
34 V. Blum, R. Gehrke, F. Hanke, P. Havu, V. Havu, X. Ren, K. Reuter and M. Scheffler, *Comput. Phys. Commun.*, 2009, **180**, 2175–2196.
35 X. Ren, P. Rinke, V. Blum, J. Wieferink, A. Tkatchenko, A. Sanfilippo, K. Reuter and M. Scheffler, *New J. Phys.*, 2012, **14**, 053020–.
36 S. Cahangirov, M. Topsakal, E. Aktürk, H. Şahin and S. Ciraci, *Phys. Rev. Lett.*, 2009, **102**, 236804.
37 E. Cadelano, P. L. Palla, S. Giordano and L. Colombo, *Phys. Rev. B*, 2010, **82**, 235414.
38 Z. Zhang, X. Liu, B. I. Yakobson and W. Guo, *J. Am. Chem. Soc.*, 2012, **134**, 19326–19329.
39 Z. Zhang, Y. Yang, E. S. Penev and B. I. Yakobson, *Adv. Funct. Mater.*, 2017, **27**, 1605059.
40 Q. Peng and S. De, *Nanoscale*, 2014, **6**, 12071–12079.
41 G. N. Greaves, A. L. Greer, R. S. Lakes and T. Rouxel, *Nat. Mater.*, 2011, **10**, 823–837.
42 Y. Wang and Y. Ding, *Phys. Status Solidi RRL*, 2013, **7**, 410–413.
43 J. Qiao, X. Kong, Z.-X. Hu, F. Yang and W. Ji, *Nat. Commun.*, 2014, **5**, 4475.
44 S. Zhang, M. Xie, F. Li, Z. Yan, Y. Li, E. Kan, W. Liu, Z. Chen and H. Zeng, *Angew. Chem.*, 2016, **128**, 1698–1701.
45 F. Li, X. Liu, Y. Wang and Y. Li, *J. Mater. Chem. C*, 2016, **4**, 2155–2159.
46 W. Zhang, Z. Huang, W. Zhang and Y. Li, *Nano Res.*, 2014, **7**, 1731–1737.
47 Z. Huang, W. Zhang and W. Zhang, *Materials*, 2016, **9**, 716.
48 A. Lherbier, A. R. Botello-Mendez and J.-C. Charlier, *2D Mater.*, 2016, **3**, 045006.

Physical Chemistry Chemical Physics Accepted Manuscript

View Article Online
DOI: 10.1039/C7CP03250A

49 R. RoldÃąn, A. Castellanos-Gomez, E. Cappelluti and F. Guinea, *J. Phys.: Condens. Matter*, 2015, **27**, 313201.

Published on 19 June 2017. Downloaded by University of Arizona on 19/06/2017 13:21:07.

Physical Chemistry Chemical Physics Accepted Manuscript